発表者氏名	論文タイトル名	発表誌名	巻号	ページ	出版年
稲田有史，中村達雄，諸井慶七郎，森本　茂	神経因性疼痛ならびにCRPS (Complex regional pain syndrome) に対する生体内再生治療	末梢神経	17	325～327	2006
萩原明於，阪倉長平，大辻英吾，山岸久一，中村達雄，清水慶彦	癌治療における神経再生の応用	再生医療	5	99～103	2006
大森孝一，多田靖宏，松塚　崇，野本幸男，鈴木輝久，中村達雄，金丸眞一，安里　亮，山下　勝，田中信三	喉頭・気管狭窄の再生治療	日本気管食道科学会会報	57(2)	153～154	2006
Omori K, Nakamura T, Kanemaru S, Asato R, Yamashita M, Tanaka S, Magrufov A, Ito J, Shimizu Y	Regenerative medicine of the trachea: The first human case	Ann Otol Rhinol Laryngol	114(6)	429～433	2005
Yokoyama S, Kano M, Watanabe M, Ogawa H, Omori K	Morphological and histologic examination of the epiglottis: Implications for improving epiglottic closure technique	Ann Otol Rhinol Laryngol	115(1)	23～29	2006
Liu K, Kozono D, Kato Y, Agre P, Hazama A, Yasui M.	Conversion of aquaporin 6 from an anion channel to a water-selective channel by asingle amino acid substitution	Proc NatlAcad Sci	102(6)	2192～2197	2005
Morino S, Nakamura T, Toba T, Takahashi M, Kushibiki T, Tabata Y, Simizu Y	Fibroblast growth factor-2 indues recovery of pulmonary blood flow in canine emphysema models	Laboratory and Animal Investigations	128	920～926	2005
Inada Y, Morimoto S, Moroi K, Endo K, Nakamura T	Surgical relief of causalgia with an artificial nerve guide tube: Successful surgical treatment of causalgia (Complex Regional Pain Syndrome Type II) by in situ tissue engineering with a polyglycolic acid-collagen tube	Pain	117	251～258	2005
Lynn AK, Nakamura T, Patel N, Porter AE, Renouf AC, Laity PR, Best SM, Cameron RE, Shimizu Y, Bonfield W	Composition-controlled nanocomposites of apatite and collagen incorporating silicon as an osseopromotive agent	J Biomed Mater Res	74A	447～453	2005
Fukuda S, Nakamura T, Kishigami Y, Endo K, Azuma T, Fujikawa T, Tsutsumi S, Shimizu Y	New canine spinal cord injury model free from laminectomy	Brain Research Protocols	14	171～180	2005
Kanemaru S, Nakamura T, Omori K, Magrufov A, Yamashita M, Ito J	Regeneration of mastoid air cells in clinical applications by in situ tissue engineering	Laryngoscope	115(2)	253～258	2005
Kanemaru S, Nakamura T, Yamashita M, Magrufov A, Kita T, Tamaki H, Tamura Y, Iguchi F, Kim TS, Kishimoto M, Omori K, Ito J	Destiny of autologous bone marrow-derived stromal cells implanted in the vocal fold	Ann Otol Rhinol Laryngol	114(12)	907～912	2005

発表者氏名	論文タイトル名	発表誌名	巻号	ページ	出版年
大森孝一，中村達雄，金丸眞一，安里　亮，山下 勝，清水慶彦	〔肺病変の修復・再生へのアプローチ〕組織工学からみた臓器再生 －気管・気管支の再生治療－	日本臨床麻酔学会誌	25(3)	310～315	2005
大森孝一	再生医療の現状と今後の展開	平成17年度福島県国保地域医療学会	抄録集	83～101	2006
多田靖宏，野本幸男，鈴木輝久，大森孝一	気道の再生	喉頭	17(2)	84～88	2005
中村達雄	＜特集 肺の再生医療～現状と展望＞気道の再生	呼吸と循環	53(2)	119～125	2005
野田澤俊介，中村達雄，清水慶彦，瀧川敏算	メッシュ型人工気管の力学特性	材料	54(1)	85～89	2005
高橋　充，加藤治文，中村達雄，清水慶彦	＜特集 肺の再生医療～現状と展望＞EPC による肺高血圧の治療	呼吸と循環	53(2)	159～165	2005
中原　貴，中村達雄，小林英三郎，呉本晃一，松野智宣，田畑泰彦，江藤一洋，清水慶彦	歯根膜由来細胞播種による歯周組織の In situ ティッシュ・エンジニアリング	歯科臨床研究	2	28～34	2005
金丸眞一	頭頸部領域の再生医療	日本耳鼻咽喉科学会会報	108(4)	330～331	2005
金丸眞一	難治性中耳炎に対する再生医学アプローチ　－in situ tissue engineering による乳突蜂巣再生の試み－	Otology Japan	15	195～202	2005
金丸眞一	頭頸部領域の再生医療	頭頸部癌	31(3)	402～407	2005
金丸眞一	人工神経チューブによる神経再生医療	喉頭	17(2)	84～88	2005
金丸眞一	＜トピックス＞頭頸部領域の再生医療	日本耳鼻咽喉科学会専門医通信	85号	28～29	2005

報道

医療材移植，気道を再生	日本経済新聞	2007年（平成19年）3月26日（月）日刊

Ⅲ．研究成果の刊行物・別刷

Available online at www.sciencedirect.com
ScienceDirect
Biochemical and Biophysical Research Communications 352 (2007) 12–16
BBRC
www.elsevier.com/locate/ybbrc

Molecular cloning and characterization of mouse aquaporin 6

Hiroaki Nagase [a,1], Johan Ågren [a,2], Akiko Saito [b], Kun Liu [a,3], Peter Agre [a,4], Akihiro Hazama [b], Masato Yasui [a,*]

[a] *Department of Biological Chemistry, Johns Hopkins University School of Medicine, 725 N. Wolfe St. Baltimore, MD 21205-2185, USA*
[b] *Department of Physiology, Fukushima Medical University School of Medicine, 1 Hikarigaoka, Fukushima City, 960-1247, Japan*

Received 15 October 2006
Available online 30 October 2006

Abstract

In the rat kidney, aquaporin (AQP) 6 is localized in the intracellular vesicle membranes of type-A intercalated cells of the collecting duct; mouse AQP6 (mAQP6) has not been characterized. Although mAQP6 was originally cloned from cDNA in a mouse cerebellum library (GenBank NM 175087), we have independently cloned a cDNA encoding mAQP6 from an adult kidney cDNA library (C57BL/6J strain). We identified two different spliced variants of mAQP6: mAQP6a and mAQP6b. The mAQP6a isoform is almost identical to that of rat AQP6, whereas mAQP6b is identical to that reported in the mouse cerebellum library mentioned above. We found that the mRNA expression of these two spliced variants is regulated in a tissue-specific and age-dependent manner. Functional analyses of water and ion permeation revealed that mAQP6a functions like rat AQP6 and that mAQP6b does not function as either a water channel or an ion channel under our experimental conditions.

Keywords: Aquaporin; Splice variant

The aquaporins (AQPs) are a family of membrane proteins that largely function as water channels [1]. In mammals, 13 members of the AQP family (AQP0-12) have been reported [2]. AQP6 has been isolated from rat and human kidneys [3,4], and in rat studies we have shown that AQP6 is functionally distinct from other known AQPs in the following ways. First, AQP6 is localized in intracellular membranes in type-A intercalated cells of the kidney [5]. Second, AQP6 functions not as a water channel but as an anion channel [5–7]: ion permeability, including that of hydronium ions, is not a general feature of AQPs [7,8]. Third, AQP6 is activated by Hg^{2+}, a well-known water channel inhibitor [1]. AQP6 has also been cloned from mouse cDNA (GenBank NM 175087) derived from the cerebellum. Interestingly, we found that the C-terminal domain of this clone exhibits no significant homology to known sequences of rat or human AQP6; also, no rat or human AQP6 has been reported in the cerebellum. Furthermore, no studies to date have examined the function of mouse AQP6 (mAQP6). To address these issues and provide a foundation for further studies of AQP6, we independently cloned mAQP6 from an adult kidney cDNA library (C57BL/6J strain). We identified two spliced variants of mAQP6. The two isoforms display distinct tissue-specific distribution, developmental regulation, and functional characteristics.

Materials and methods

Isolation of mAQP6 isoforms. Primers for the full-length of the mAQP6 coding region were designed from the cDNA retrieved from GenBank

* Corresponding author. Present address: Department of Pharmacology, Keio University School of Medicine, 35 Shinanomachi, Shinjuku, Tokyo 160-8582, Japan. Fax: +81 3 3359 8889.
E-mail address: myasui@sc.itc.keio.ac.jp (M. Yasui).
[1] Present address: Deaprtment of Pediatric Neurology, Kobe Children's Hospital, Kobe, Hyogo, Japan.
[2] Present address: Department of Women's and Children's Health, Uppsala University, Uppsala, Sweden.
[3] Present address: Trimgen Genetic Diagnostics, Sparks, MD, USA.
[4] Present address: Department of Cell Biology, Duke University School of Medicine, Durham, NC, USA.

0006-291X/$ - see front matter © 2006 Elsevier Inc. All rights reserved.
doi:10.1016/j.bbrc.2006.10.110

(Accession No. NM 175087) with the *Eco*RI site as the upstream primer and the *Nhe*I site as the downstream primer. The sequence of the upstream primer was 5′-ATAGAATTCCATGGAGCCAGGGCTGTGTAGC-3′ and that of the downstream primer was 5′-AATAGCTAGCTCAG CAAAGGCCAAGCGTGAATG-3′. All animal experiments were conducted under protocols approved by the Johns Hopkins Animal Care and Use Committee. Total RNA was extracted from the kidneys of adult (3–4-month-old) C57BL/6J mice using the RNeasy kit with optional DNase treatment (Qiagen, Valencia, CA). An aliquot of 5 μg of total RNA was then used for cDNA synthesis with the SuperScript First-Strand Synthesis System for RT-PCR (Invitrogen, Carlsbad, CA), and 2.5 μL of the resulting cDNAs was subsequently amplified using the Expand High Fidelity PCR system (Roche Applied Science, Penzberg, Germany). All PCR products were purified with a Qiaquick Gel Extraction Kit (Qiagen) and subcloned into the multiple cloning regions of pXβG-myc and pcXβG3 vectors at the *Eco*RI and *Nhe*I sites. The pcXβG3 vector had been constructed by cloning the *Xenopus* β-globin 5′- and 3′- untranslated regions into the pcDNA3 vector (and was kindly supplied by Michael Caterina, Johns Hopkins University, Baltimore, MD, USA). The pXβG-myc vector was constructed by adding a c-myc tag at the *Bgl*I site of the pXβG vector. Sequencing was used to verify the DNA sequence of the constructs.

Analysis of mAQP6 mRNA expression using RT-PCR. RNA extraction and RT-PCR were performed as described above using cerebella and kidneys from 1-day-old (P1) and adult mice. This time 2 μL of the resulting cDNAs was amplified with primers synthesized according to the sequence of mAQP6 cDNA. The upstream primer used for mAQP6 cDNA was 5′-ACTGGCTGTTCCATGAACCC-3′, and the downstream primer was 5′-AGGAAGTGGCCAGGAGGTACT-3′. The PCR were cycled 40 times, using a 1-min, 94 °C denaturing step; a 1-min, 61 °C annealing step; and a 1-min, 72 °C extension step. The PCR products were visualized by ethidium bromide staining and electrophoresis in 2% agarose.

Expression in oocytes and measurement of P_f. Capped cRNAs were synthesized in vitro from *Xba*I-linearized pcXβG3 plasmids with T7 RNA polymerase and purified with the RNeasy kit (Qiagen). Five nanograms (50 nL) of cRNA or 50 nL of diethyl pyrocarbonate-treated water was injected into defolliculated mature *Xenopus laevis* oocytes (controls). The oocytes were incubated for 2–3 days at 18 °C in 200 mOsm modified Barth's solution (MBS). An oocyte-swelling assay was used to measure osmotic water permeability (P_f) was measured from the time course of oocytes swelling in response to a 3-fold dilution of MBS with distilled water as in previous studies [9]. For Hg^{2+} studies, oocytes were preincubated for 5 min in 200 mOsm MBS containing 0.5 mM $HgCl_2$ before the swelling assay, whereas the controls were preincubated without $HgCl_2$.

Oocyte immunofluorescence and confocal microscopy. Three days after injection oocytes were incubated in fixing solution (80 mM Pipes, pH 6.8, 5 mM EGTA, 1 mM $MgCl_2$, 3.7% formaldehyde, and 0.2% Triton X-100) at room temperature for 4 h, transferred to methanol at −20 °C for 24 h, equilibrated in PBS at room temperature for 2 h, incubated in PBS with 100 mM $NaBH_4$ at room temperature for 24 h, and bisected with blades. The oocytes were blocked by 2% BSA in PBS for 1 h at room temperature, incubated at 4 °C sequentially with rabbit anti-AQP6 antibody [10] and Alexa Fluor 488 goat anti-rabbit IgG (Invitrogen) in blocking buffer (each for 24 h), and mounted in Fluoromount-G (SouthernBiotech, Birmingham, AL, USA). Micrographs were obtained with a confocal laser-scanning microscope (UltraView LCI, Perkin-Elmer, Wellesley, MA, USA).

Oocyte membrane extraction and immunoblotting. Ten oocytes were homogenized by pipetting them up and down in hypotonic lysis buffer (7.5 mM sodium phosphate, 1 mM EDTA, pH 7.5) including a protease inhibitor mixture (Sigma–Aldrich, St. Louis, MO, USA). The oocyte yolk was removed by discarding the pellet after centrifugation at 735*g* and 4 °C for 10 min. The supernatant was centrifuged again at 200,000*g* and 4 °C for 1 h; the membrane was harvested by collecting the pellet. The oocyte membrane was solubilized with 2% SDS, normalized by total protein amount following the BCA method (Pierce, Rockford, IL, USA), and subjected to 12% SDS–PAGE. The proteins were transferred to a poly-vinylidene-difluoride) membrane, probed with a rabbit anti-rat AQP6 antibody and a horseradish peroxidase-conjugated donkey anti-rabbit IgG (Amersham Biosciences, Pittsburgh, PA, USA). An enhanced chemiluminescence detection system (ECL-plus, Amersham Biosciences) was used to visualize the specific immunoreactive proteins by exposure to autoradiographic films.

Electrophysiological measurements of oocytes were performed with iso-osmotic. NaCl solution (100 mM NaCl, 2 mM KCl, 1 mM $MgCl_2$, and 5 mM Hepes, pH 7.5) or iso-osmotic $NaNO_3$ solution (100 mM $NaNO_3$, 2 mM KCl, 1 mM $MgCl_2$, and 5 mM Hepes, pH 7.5). The membrane potential of oocytes was controlled by the two-microelectrode voltage clamp technique. The command voltage was applied with a two-microelectrode voltage clamp amplifier (Axoclamp-2A, Axon Instruments, Foster City, CA) controlled by an IBM-compatible computer running pCLAMP software (Axon Instruments). Current signals were sampled at 100 μs. In most experiments the membrane potential was held at $V_{hold} = -50$ mV. To determine the current–voltage relationship, the membrane potential was rapidly stepped up from the holding potential to a series of values generating between +50 and −130 mV, each differing by 20 mV. The pulse duration was 100 ms, and currents from 10 runs were averaged to reduce noise. All measurements were performed at room temperature.

Results

By RT-PCR experiments using mouse kidney cDNA as a template, we obtained two different full-length cDNA fragments. One of them (named mAQP6a) (GenBank DQ 826418) was almost identical to rAQP6, whereas the other clone (named mAQP6b) was identical to the previously reported mAQP6 (GenBank NM 175087). The mAQP6a cDNA results from a retention of intron 4, creating a novel 3′ end (Fig. 1A). Nucleotide sequencing analysis revealed that the mAQP6 gene encodes proteins with 276 and 293 amino acid residues and that the difference is observed only at the C-terminus (Fig. 1B). The mAQP6b C-terminal domain exhibits no significant homology to known sequences from other AQPs.

Expression of mAQP6 in the cerebellum and kidney

To investigate the age-related and tissue-specific expression of mAQP6a and mAQP6b, we performed RT-PCR with primers that are designed to amplify 727-bp and 364-bp fragments for mAQP6a and mAQP6b, respectively (Fig. 2). In the cerebellum, mAQP6b was detected only in P1 mice, from which mAQP6b was originally cloned, whereas mAQP6a was expressed not in the P1 but in the adult cerebellum. In the kidney, mAQP6a, and mAQP6b were expressed in both P1 and adult mice. Expression of mAQP6a was higher in adult mice, in both the cerebellum and kidney.

Functional studies

The functional properties of mAQP6 were evaluated by expression in *Xenopus* oocytes. Swelling was monitored after the oocytes had been transferred from 200 to 70 mOsm modified Barth's solution, and the coefficients of osmotic water permeability (P_f) were calculated. Like

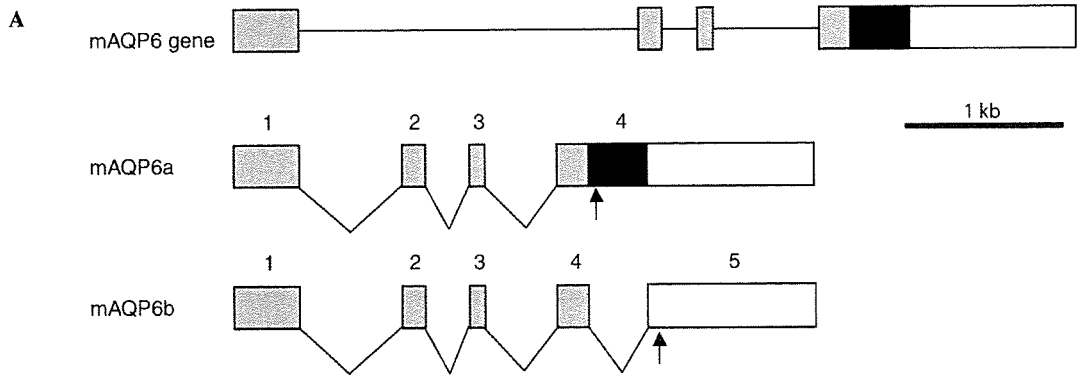

B

```
rAQP6    1  MEPGLCNRAYLLVGGLWTAISKALFAEFLATGLYVFFGVGSVLPWPVALP  50  rAQP6
mAQP6a   1  MEPGLCSRAYLLVGGLWTAISKALFAEFLATGLYVFFGVGSVLPWPVALP  50  mAQP6a
mAQP6b   1  MEPGLCSRAYLLVGGLWTAISKALFAEFLATGLYVFFGVGSVLPWPVALP  50  mAQP6b

rAQP6   51  SVLQVAITFNLATATAVQISWKTSGAHANPAVTLAYLVGSHISLPRAVAY  100  rAQP6
mAQP6a  51  SVLQIAITFNLATATAVQISWKTSGAHANPAVTLAYLVGSHISLPRAMAY  100  mAQP6a
mAQP6b  51  SVLQIAITFNLATATAVQISWKTSGAHANPAVTLAYLVGSHISLPRAMAY  100  mAQP6b

rAQP6   101 IAAQLAGATVGAALLYGVTPGGVRETLGVNVVHNSTSTGQAVAVELVLTL  150  rAQP6
mAQP6a  101 IAAQLAGATAGAALLYGVTPGGIRETLGVNVVHNSTSTGQAVAVELVLTL  150  mAQP6a
mAQP6b  101 IAAQLAGATAGAALLYGVTPGGIRETLGVNVVHNSTSTGQAVAVELVLTL  150  mAQP6b

rAQP6   151 QLVLCVFASMDSRQTLGSPAAMIGTSVALGHLIGIYFTGCSMNPARSFGP  200  rAQP6
mAQP6a  151 QLVLCVFASMDGRQTLASPAAMIGTSVALGHLIGIYFTGCSMNPARSFGP  200  mAQP6a
mAQP6b  151 QLVLCVFASMDGRQTLASPAAMIGTSVALGHLIGIYFTGCSMNPARSFGP  200  mAQP6b

rAQP6   201 AVIVGKFAVHWIFWVGPLTGAVLASLIYNFILFPDTKTVAQRLAILVGTT  250  rAQP6
mAQP6a  201 AVIVGKFAVHWIFWVGPLTGAVLASLIYNFILFPDTKTVAQRLAILVGTT  250  mAQP6a
mAQP6b  201 AVIVGKFAVHWIFWVGPLTGAVLASLIYNFILFPDTKTVAQRLAILVGTT  250  mAQP6b

rAQP6   251 KVEKVVDLEPQKKESQTNSEDTEVSV                      276  rAQP6
mAQP6a  251 KVEKVVDLEPQKKESQTNSEDTEVSV                      276  mAQP6a
mAQP6b  251 KVEKVVDLEPQKKESQTNSEDTECLTSPCEEAVRSFSFTLGLC     293  mAQP6b
```

Fig. 1. Isolation of mAQP6 splicing variants. (A) Exon–intron organization of the mouse AQP6 gene. A segment of the genomic *AQP6* clone is shown at the top of the figure. The gray rectangles represent common translated regions of AQP6. Exon 4 of mAQP6a contains a black rectangle with a stop codon in it (arrow). mAQP6b has another intron (intron 4) and exon 5; the stop codon is in exon 5. (B) Sequence alignments of rat AQP6, mAQP6a, and mAQP6b. The blue residues are identical. Red NPAs are a motif of AQPs. (For interpretation of the references to colour in this figure legend, the reader is referred to the web version of this article.)

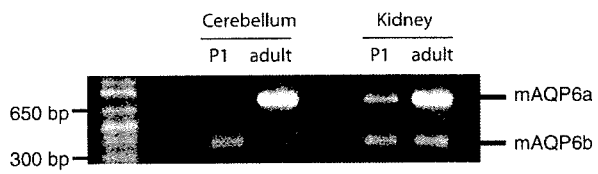

Fig. 2. Developmental regulation of mAQP6 transcripts. RT-PCR analysis of mAQP6 expression in the mouse kidney and cerebellum. Total RNA of different developmental points; neonatal (P1) and adult mice subjected to RT-PCR using specific primers for mAQP6.

rAQP6, mAQP6a has low water permeability, which is activated by Hg^{2+} (Fig. 3A). On the other hand, Hg^{2+} does not activate mAQP6b, which also has low basal water permeability. We evaluated the ionic permeation of oocytes expressing mAQP6 using a two-electrode voltage clamp. Oocytes expressing mAQP6a exhibit current under Hg^{2+} treatment, which is also the case with of oocytes expressing rAQP6 (Fig. 3B). On the other hand, of oocytes expressing mAQP6b did not exhibit any current either with or without Hg^{2+} treatment. Confocal microscopy demonstrated that both mAQP6a and mAQP6b are located at the oocyte plasma membrane (Fig. 4A). It should be noted that the anti-AQP6 antibody recognized a 30-kDa and a 28-kDa band from oocytes into which mAQP6a had been injected and also recognized a 31-kDa and a 29-kDa band from oocytes into which mAQP6b had been injected (Fig. 4B).

Discussion

We have previously characterized rat AQP6 [5–7,10] and found that it is localized in the acid-secreting cells of the renal collecting ducts [10] and functions as an anion channel [5–7]. Mouse AQP6 was cloned from a cerebellum library during a large-scale full-length cDNA expression analysis in mice carried out by RIKEN as part of the FANTOM project (GenBank NM 175087) [11,12]. The FANTOM project represents one of the most comprehensive surveys of a mammalian transcriptome using a full-length cDNA set. However, as was pointed out at the time, it is necessary to perform experimental analyses to verify

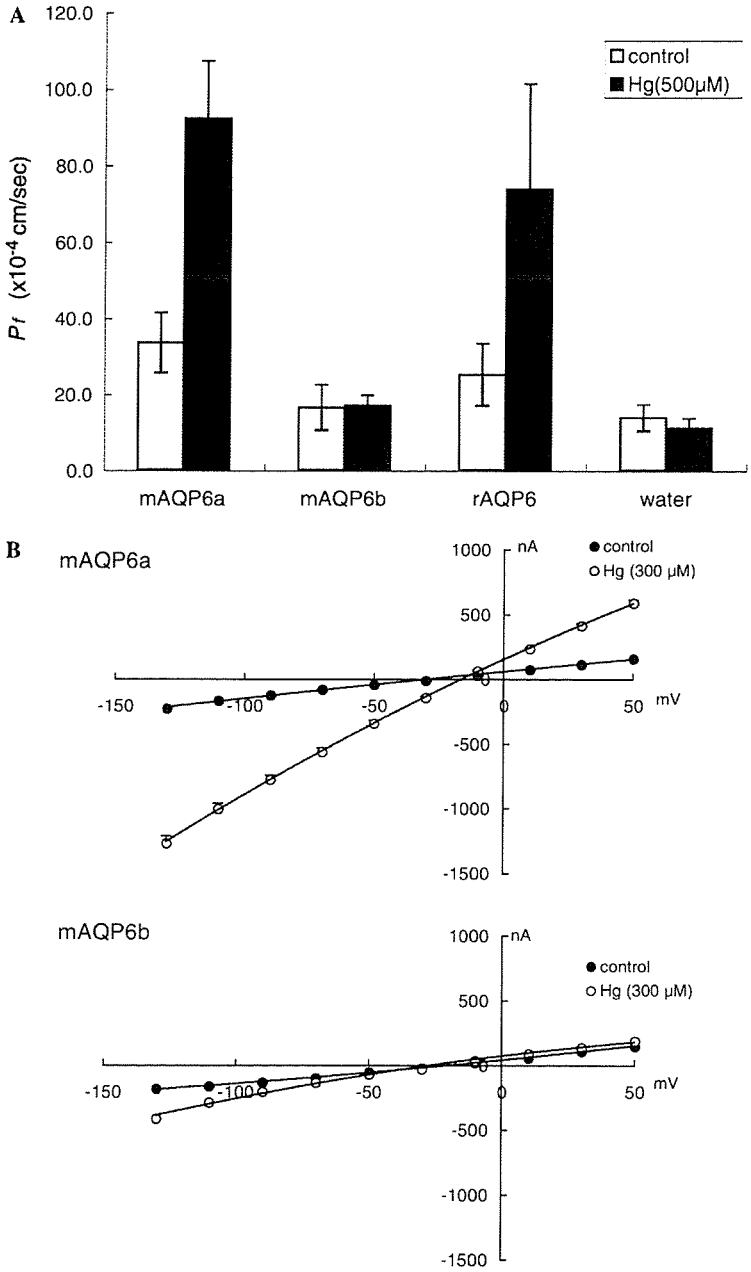

Fig. 3. (A) The coefficient of osmotic water permeability (P_f) of mAQP6a, mAQP6b, and rAQP6. Mercury treatment activated water permeability in mAQP6a and rAQP6 but not in mAQP6b. (B) Electrophysiological analyses of mAQP6a and mAQP6b. One-volt curves between +50 and −130 mV were plotted for data obtained from mAQP6a (upper panel) and mAQP6b (lower panel) oocytes. Electrophysiological experiments were performed with a two-electrode voltage clamp system. The membrane potential was held at −50 mV and rapidly stepped up to test potentials from −50 to −130 mV at 20-mV intervals. Currents at each voltage were measured with pClamp software.

the functions of genes predicted by computational analyses. The primary sequence revealed that this clone is very different from that of rat or human AQP6. In this study we independently cloned and characterized mAQP6. We found that a new spliced variant of mAQP6 resulted from intron retention and an alternative in-frame stop codon. The new isoform (termed mAQP6a) is almost identical to rat AQP6, whereas the other clone (here called mAQP6b), which has a different C-terminal amino acid, is identical to the one reported in the RIKEN study. Interestingly, we found that both function and distribution differ between mAQP6a and mAQP6b. Sequence homology showed that when expressed in oocytes mAQP6a, like rat AQP6, is activated by Hg^{2+} and permeated by ions, whereas mAQP6b does not function either as a water channel or an ion channel. The abundance of mAQP6b in neonatal mouse

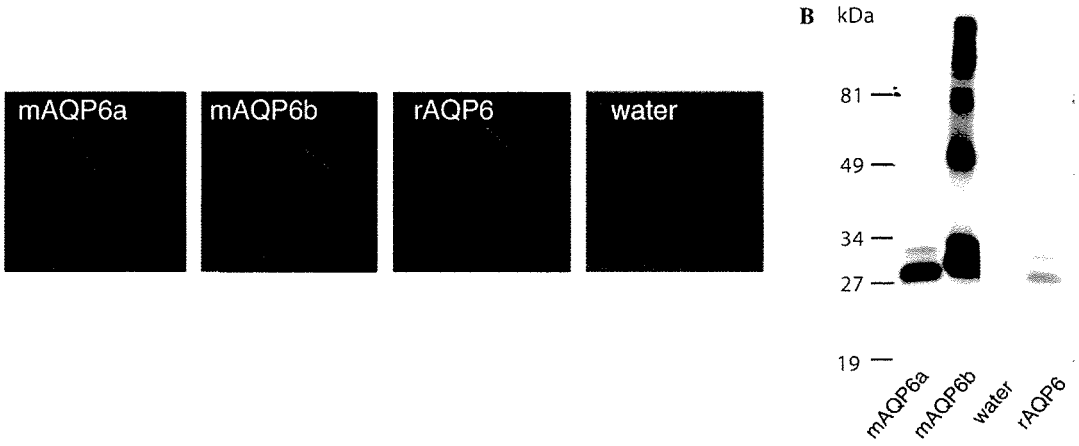

Fig. 4. mAQP6/rAQP6 expressed in oocytes. (A) Confocal microscope images of oocytes into which water, mAQP6a, mAQP6b, or rAQP6 had been injected. The oocytes were stained with an anti-rat AQP6 antibody. (B) Immunoblotting of membrane fractions from oocytes into which mAQP6a, mAQP6b, water, or rAQP6 had been injected.

cerebella is consistent with the isolation of the previously reported mouse AQP6 clone from the cerebella of neonatal mice.

We also found that the expression of the mRNA of these two splicing variants is regulated in a tissue-specific and age-related manner, suggesting that mAQP6 may be important during development. The expression of mAQP6a and mAQP6b in the cerebellum is provocative. Immunocytochemical studies with mAQP6-specific antibodies will be needed to determine the physiological relevance of AQP6 to cerebellar function.

Functional analysis revealed that mAQP6a functions as an anion channel, as does rat AQP6. Although mAQP6b was expressed in the plasma membranes of oocytes, we could not demonstrate any water or ion transport. Thus, the biological function of mAQP6b remains unclear. The C-terminus of mAQP6b has a putative casein kinase II phosphorylation site at Ser 277, which may regulate channel gating. One could speculate that mAQP6b forms a heterologous oligomer with mAQP6a, which may have a dominant negative effect on both proteins. However, when mAQP6a and mAQP6b were expressed together in oocytes, no dominant negative effects were detected (data not shown).

Our immunofluorescence studies revealed that both mAQP6a and mAQP6b are expressed in the plasma membranes of oocytes. Although the C-terminus of rat AQP6 is presumably less important for trafficking than is the N-terminus [6], these two isoforms might traffic differently when expressed in mammalian cells. To clarify the precise distribution of mAQP6b, we plan to develop an antibody that recognizes mAQP6b but not mAQP6a. mAQP6b may have distinct cellular distributions and functions during development.

Acknowledgments

This work was supported by a Grant DK065098 from National Institution of Health, and Ministry of Education, Science, Sports and Culture. Grant-in Aid for Scientific Research (C) 15590902, Japan.

References

[1] P. Agre, L.S. King, M. Yasui, W.B. Guggino, O.P. Ottersen, Y. Fujiyoshi, A. Engel, S. Nielsen, Aquaporin water channels—from atomic structure to clinical medicine, J. Physiol. 542 (2002) 3–16.
[2] T. Itoh, T. Rai, M. Kuwahara, S.B. Ko, S. Uchida, S. Sasaki, K. Ishibashi, Identification of a novel aquaporin, AQP12, expressed in pancreatic acinar cells, Biochem. Biophys. Res. Commun. 330 (2005) 832–838.
[3] T. Ma, A. Frigeri, W. Skach, A.S. Verkman, Cloning of a novel rat kidney cDNA homologous to CHIP28 and WCH-CD water channels, Biochem. Biophys. Res. Commun. 197 (1993) 654–659.
[4] T. Ma, B. Yang, W.L. Kuo, A.S. Verkman, cDNA cloning and gene structure of a novel water channel expressed exclusively in human kidney: evidence for a gene cluster of aquaporins at chromosome locus 12q13, Genomics 35 (1996) 543–550.
[5] M. Yasui, A. Hazama, T.H. Kwon, S. Nielsen, W.B. Guggino, P. Agre, Rapid gating and anion permeability of an intracellular aquaporin, Nature 402 (1999) 184–187.
[6] M. Ikeda, E. Beitz, D. Kozono, W.B. Guggino, P. Agre, M. Yasui, Characterization of aquaporin-6 as a nitrate channel in mammalian cells. Requirement of pore-lining residue threonine 63, J. Biol. Chem. 277 (2002) 39873–39879.
[7] A. Hazama, D. Kozono, W.B. Guggino, P. Agre, M. Yasui, Ion permeation of AQP6 water channel protein. Single channel recordings after Hg^{2+} activation, J. Biol. Chem. 277 (2002) 29224–29230.
[8] N. Chakrabarti, B. Roux, R. Pomes, Structural determinants of proton blockage in aquaporins, J. Mol. Biol. 343 (2004) 493–510.
[9] G.M. Preston, T.P. Carroll, W.B. Guggino, P. Agre, Appearance of water channels in *Xenopus* oocytes expressing red cell CHIP28 protein, Science 256 (1992) 385–387.
[10] M. Yasui, T.H. Kwon, M.A. Knepper, S. Nielsen, P. Agre, Aquaporin-6: an intracellular vesicle water channel protein in renal epithelia, Proc. Natl. Acad. Sci. USA 96 (1999) 5808–5813.
[11] J. Kawai et al., Functional annotation of a full-length mouse cDNA collection, Nature 409 (2001) 685–690.
[12] Y. Okazaki et al., Analysis of the mouse transcriptome based on functional annotation of 60,770 full-length cDNAs, Nature 420 (2002) 563–573.

Acta Oto-Laryngologica 2007; Suppl 557: 66–72

informa
healthcare

Experimental regeneration of canine larynx: a trial with tissue engineering techniques

MASARU YAMASHITA[1], KOICHI OMORI[2], SHIN-ICHI KANEMARU[1], AKHMAR MAGRUFOV[1], YOSHIHIRO TAMURA[1], HIROO UMEDA[1], MASANAO KISHIMOTO[1], TATSUO NAKAMURA[3], & JUICHI ITO[1]

[1]*Department of Otolaryngology-Head and Neck Surgery, Graduate School of Medicine, Kyoto University, Kyoto,* [2]*Department of Otolaryngology, Fukushima Medical University, Fukushima and* [3]*Department of Bioartificial Organs, Institute for Frontier Medical Sciences, Kyoto University, Kyoto, Japan*

Abstract

Conclusion: Since this tissue engineering technique is cost-effective and is less invasive to patients, it may replace conventional approaches in laryngeal reconstructive surgeries. *Objective:* Laryngeal cancer is one of the most prevalent cancers in the head and neck region, and frequently requires surgical resection. Although there are many ways to reconstruct the larynx after resection, donor tissue is usually required. Recently, tissue engineering techniques have become widely accepted in clinical medicine and have already been applied to some organs. This animal experiment was designed to elucidate the efficacy of laryngeal regeneration using tissue engineering technique. *Materials and methods:* A bioartificial scaffold was designed from a replica of a canine larynx. A dental cast was used to replicate the intricate inside shape of the larynx. After copying its shape on a polypropylene mesh sheet, this sheet was coated with spongy collagen from porcine skin. A hemilaryngectomy was performed on beagle dogs under general anesthesia. Then the scaffold, preclotted with a mixture of peripheral blood and bone marrow-derived stromal cells, was implanted and fixed. The postoperative status was examined fiberscopically. *Results:* On the eighth day after the operation, the surface of the implant was covered with soft tissue. Finally, the implant was completely covered with regenerated mucosa.

Keywords: *Laryngeal regeneration, tissue engineering, bioartificial scaffold, polypropylene, bone marrow-derived stromal cells*

Introduction

Although many approaches are available for laryngeal reconstruction after partial resection and physicochemical damage, such as the use of autologous tissue, allografts, and artificial materials, a reliable and standard model has yet to be established. For complete reconstruction of the larynx, anatomical configuration and functions have to be restored, rendering the task challenging.

Recently, remarkable progress has been achieved in regenerative medicine; highly differentiated tissues and certain organs can now be regenerated under appropriate conditions, using tissue engineering techniques [1–3]. These techniques routinely require three fundamental components: cells, scaffold (a cell-ingrowth transplant medium for regeneration), and growth regulation factors. Of these, the scaffold on which cells are grown is particularly important for regenerating tissues and organs.

In structure–function relationships, the larynx is not an exception in terms of its status as an organ. If an appropriate scaffold was prepared, regeneration of the larynx would be facilitated. In this study, laryngeal regeneration was attempted in dogs with a novel approach using a canine-replicated scaffold innovated with bone marrow-derived stromal cells (BSCs).

Materials and methods

Preparation of scaffolds and media for cell growth

A single sheet of polypropylene mesh with a pore size of 260 μm (Marlex mesh®; CR Bard, Billerica, MA,

Correspondence: Shin-ichi Kanemaru, MD, PhD, Department of Otolaryngology-Head and Neck Surgery, Graduate School of Medicine, Kyoto University, 54 Kawara-cho, Syogoin, Sakyo-ku, Kyoto 606-8507, Japan. Tel: +81 75 751 3346. Fax: +81 75 751 7225. E-mail: kanemaru@ent.kuhp.kyoto-u.ac.jp

ISSN 0365-5237 print/ISSN 1651-2551 online
DOI: 10.1080/00016480601068014

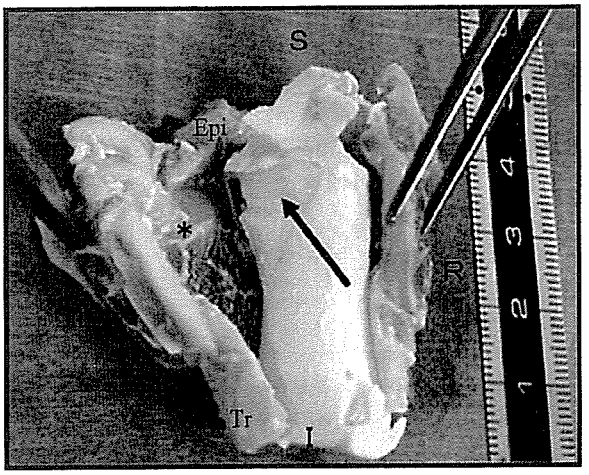

Figure 1. After the casting procedure, the cast lies on the right luminal surface of the larynx. A section was cut on the posterior side of the larynx with the left side of the larynx opened for viewing. The arrow shows an impressed shape of the left vocal fold (*) on a dental cast. Epi, epiglottis; Tr, trachea; S, superior; I, inferior; R, right; L, left.

USA) was used as the scaffold ground-framework. A female beagle dog (body weight 12 kg) employed as a control in a previous study was sacrificed, and the larynx was isolated. The shape of the larynx was then impressed with inpours from a dental cast (Neoprimestone®, Mutsumi Chemical Industries, Mie, Japan) (Figure 1). The anatomical contours were then molded accordingly on a polypropylene mesh sheet with heat (100°C, 1 h) using a drying sterilizer (SG-61, Yamato Scientific, Tokyo, Japan).

Another flat polypropylene mesh sheet (see above) was layered on the scaffold to structurally reinforce and firmly maintain its shape before fixation with fine polypropylene filaments (Figure 2A). A 1% porcine dermal atelocollagen (supplied by Nippon Meatpackers, Ibaraki, Japan) preparation comprising type I (70%) and type III (30%) collagens dissolved in aqueous hydrochloric acid (HCl, pH 3.0) was coated on both sides of the fixed polypropylene mesh sheets. After collagen-coating, freeze-drying with a freeze dryer (FDU-810, Tokyo Rikakikai, Tokyo, Japan), and cross-linkage with a vacuum dry oven (VOS-300SD, Tokyo Rikakikai) were applied to the scaffold to facilitate cellular attachment and ingrowth (Figure 2B).

Preparation of BSCs

Bone marrow extract (approx. 2 ml) obtained from the left humerus of each animal with an extractor, was placed in an 80 cm^2 culture bottle and incubated with Dulbecco's modified Eagle medium containing 10% fetal bovine serum and antibiotics (penicillin G Na 10 000 units/ml, streptomycin sulfate 10 000 μg/ml, and 25 μg/ml amphotericin B as fungizone in 0.85% saline; Invitrogen, Carlsbad, CA, USA) at 37°C under 5% CO_2 atmosphere.

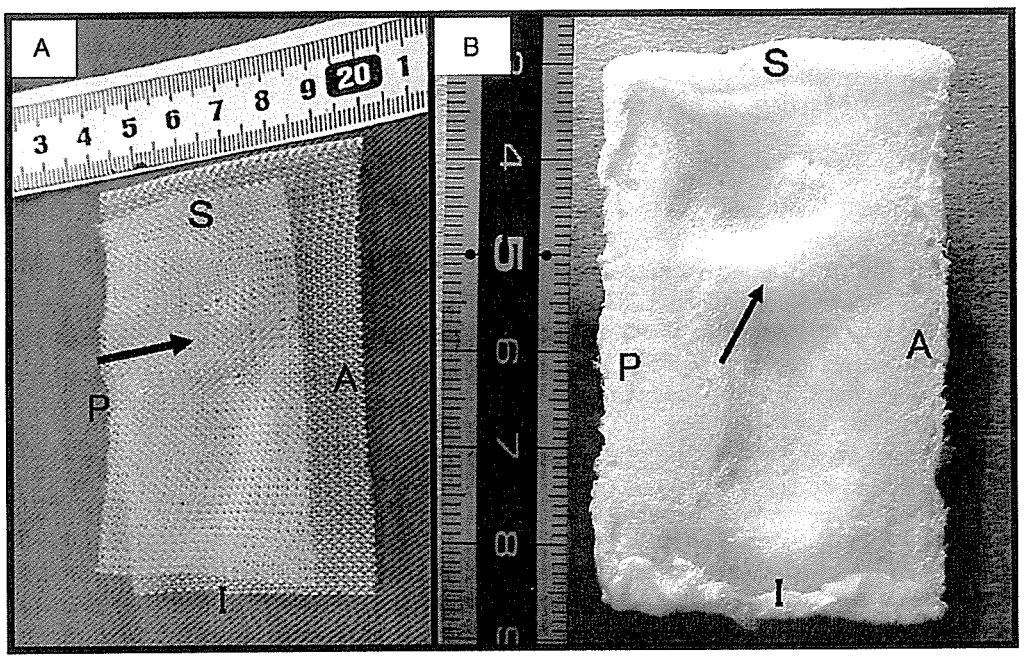

Figure 2. (A) The affected contours of a vocal fold on a polypropylene mesh are indicated by an arrow. The inner side mesh was reinforced by an overlying flat mesh sheet. (B) A luminal view of the scaffold after collagen treatment with the level of the resected vocal fold indicated by an arrow. S, superior; I, inferior; A, anterior; P, posterior.

After removal of the floating cells by aspiration, those attached on the bottom of the bottle were incubated in the fresh medium described above for 1 month without passage. Replacements of medium were regularly repeated with fresh portions at 3-day intervals. Attached cells were collected by trypsin treatment ($1.0-2.0 \times 10^6$ cells) and used as BSCs.

Animals and surgical procedures

Animal care, housing, and experimental procedures were conducted according to the Guideline for Animal Experiments of Kyoto University. Three adult beagle dogs (X, Y, and Z), each weighing 12–14 kg, were anesthetized with ketamine HCl (5.0 mg/kg; Sankyo, Tokyo, Japan) and xylazine HCl (2.0 mg/kg; Bayer, Tokyo, Japan) followed by tracheal intubation. The animals were then generally anesthetized with a mixture of oxygen, nitrous oxide, and halothane before left vertical hemilaryngectomy (Figure 3), approx. 2.5 cm × 2 cm in size, using a scalpel. A scaffold implant, preclotted with 5 ml of arterial blood containing BSCs, was trimmed according to the defect size during the operation (Figure 4). The clotting procedure rendered the implant completely infiltrated with BSCs and neutralized any air spaces from causing leakage and/or hindering cell growth. The fully prepared scaffold for each experimental animal was anastomosed according to resected boundaries of the defect and arytenoid cartilage with 3–0 absorbable sutures (Vicryl®; Ethicon, Somerville, NJ, USA) (Figure 5). Ampicillin sodium (Meiji Seika Kaisha, Tokyo, Japan) was administered (250 mg/animal; s.c.) for 3 days, followed by daily oral 500 mg doses for 2 weeks to prevent postoperative infections.

Outcome assessment

Endoscopic examinations to monitor progress of regenerative status were undertaken periodically. Anesthesia was induced with ketamine HCl and xylazine HCl (see above) to facilitate these examinations. The luminal status was examined with a video-endoscopy system consisting of a video bronchoscope (BF type 1T240, Olympus, Tokyo, Japan) and a video processor (CV-240, Olympus) with a light source (CLV-U40D, Olympus).

Images were portrayed via computed tomography (CT) performed on the operated site using a helical CT scanner system (Legato Duo, GE Yokogawa Medical Systems, Tokyo, Japan).

Results

The postoperative conditions of two dogs (X and Z) were normal, while the remaining dog (Y) died of unknown causes 4.5 months after the operation.

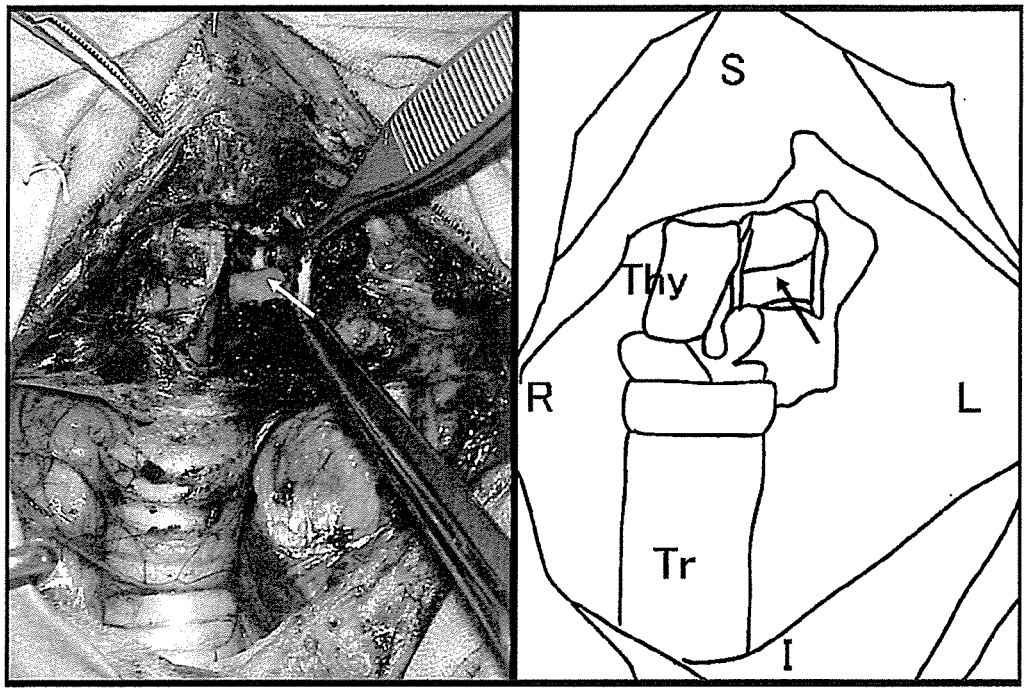

Figure 3. A left vertical hemilaryngectomy (left panel) performed on the larynx was simplified with an illustrative diagram (right panel) for reference. The arrows indicate the left vocal folds. Thy, right ala of the thyroid cartilage; Tr, trachea; S, superior; I, inferior; R, right, L, left.

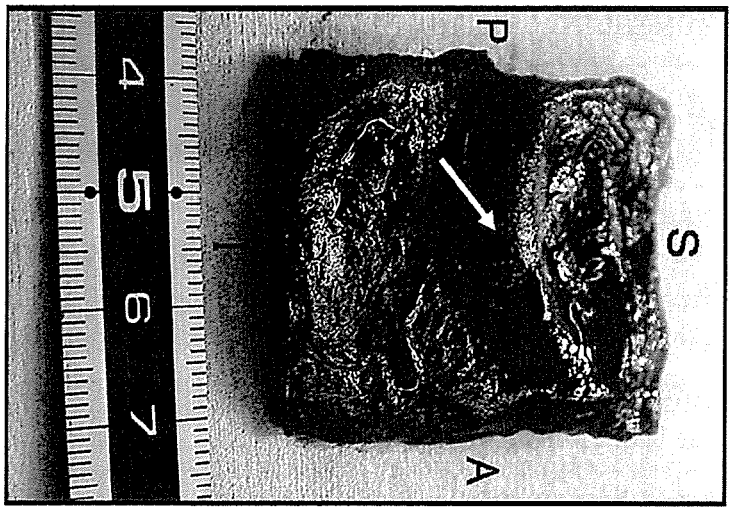

Figure 4. The level of the vocal cord after the preclotting procedure. S, superior; I, inferior; A, anterior; P, posterior.

Dog X was sacrificed 1 year after the operation. The local fiberscopic findings of the three dogs are summarized in Table I.

Fiberscopic images of operative events in dog Z (Figures 6 and 7) with typical luminal portrayals of a successfully reconstructed larynx at 20 months post-operatively (Figure 7) compared with the preoperative image of a normal larynx (Figure 6A). The preclotted and fixed scaffold implant was a good fit on the left side of the larynx immediately after the operation (Figure 6B), and the implant surface was covered with soft tissues on day 8 after operation (Figure 6C). The surface of the implant was completely proliferated with regenerated mucosal cells 3 weeks (Figure 6D), followed by structural framing of stabilized contours of the regenerated vocal fold without displacements. The bulge of the regenerated vocal fold was still maintained at 20 months after operation.

At 15 months after operation, a CT image (Figure 8) revealed a molded vocal fold, which had a contour structurally resembling the contralateral control larynx without obvious cartilage regeneration.

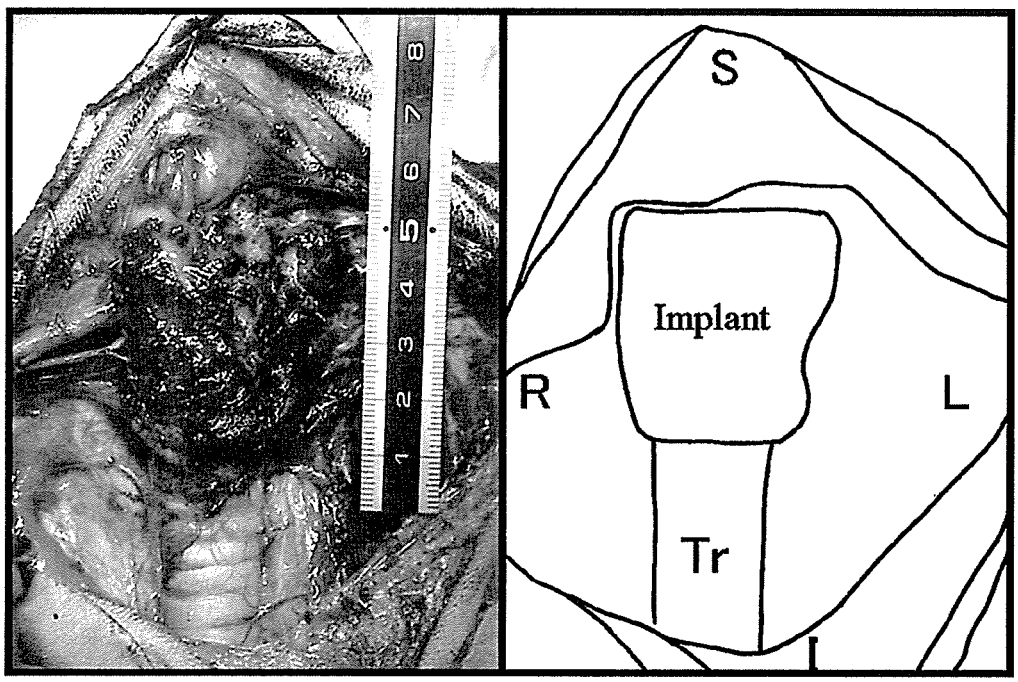

Figure 5. The larynx after implant fixation (left panel) with an illustrative diagram (right panel) for reference. Tr, trachea; S, superior; I, inferior; R, right; L, left.

Table I. Endoscopic findings.

Dog	Stenosis	Epithelialization	Granulation	Exposure of mesh
X	–	Poor	–	+
Y	–	Poor	+	+
Z	–	Good	–	–

Discussion

Various options to reconstruct the larynx after partial surgical resections and/or structural damage have been pursued for more than 50 years [4–11]. However, hitherto established treatments have remained controversial as surgeons continued to encounter inconsistent and incomplete outcomes in laryngeal reconstructions. Factors contributing to unsatisfactory outcomes include: (i) difficulty in reconstructing delicate tissues and structures (having other functions), which are anatomically located in the practically inaccessible larynx, which as a whole is influenced by movements of swallowing and vibrations of vocal cords; (ii) the organ per se is located at an impractically accessible anatomical site; and (iii) factor (i) imposes high-risk operative procedures. Although autologous tissues [4–11] and homografts [12,13] have hitherto been employed as implant materials for laryngeal reconstruction, damage inflicted on the donor site and/or the risk of donor–recipient disease transmissions warrants a more useful and a clinically more efficient approach. Moreover, in cases with tumors in the larynx, deformities of the reconstructed site render it difficult to monitor tumor recurrence. Furthermore, unintentionally inflicted cosmetic handicaps in operated patients sometimes mold unfavorable psychological outcomes that eventually overwhelm the reconstruction effort.

Regenerative medicine has recently been accepted as a useful clinical discipline that ensures and

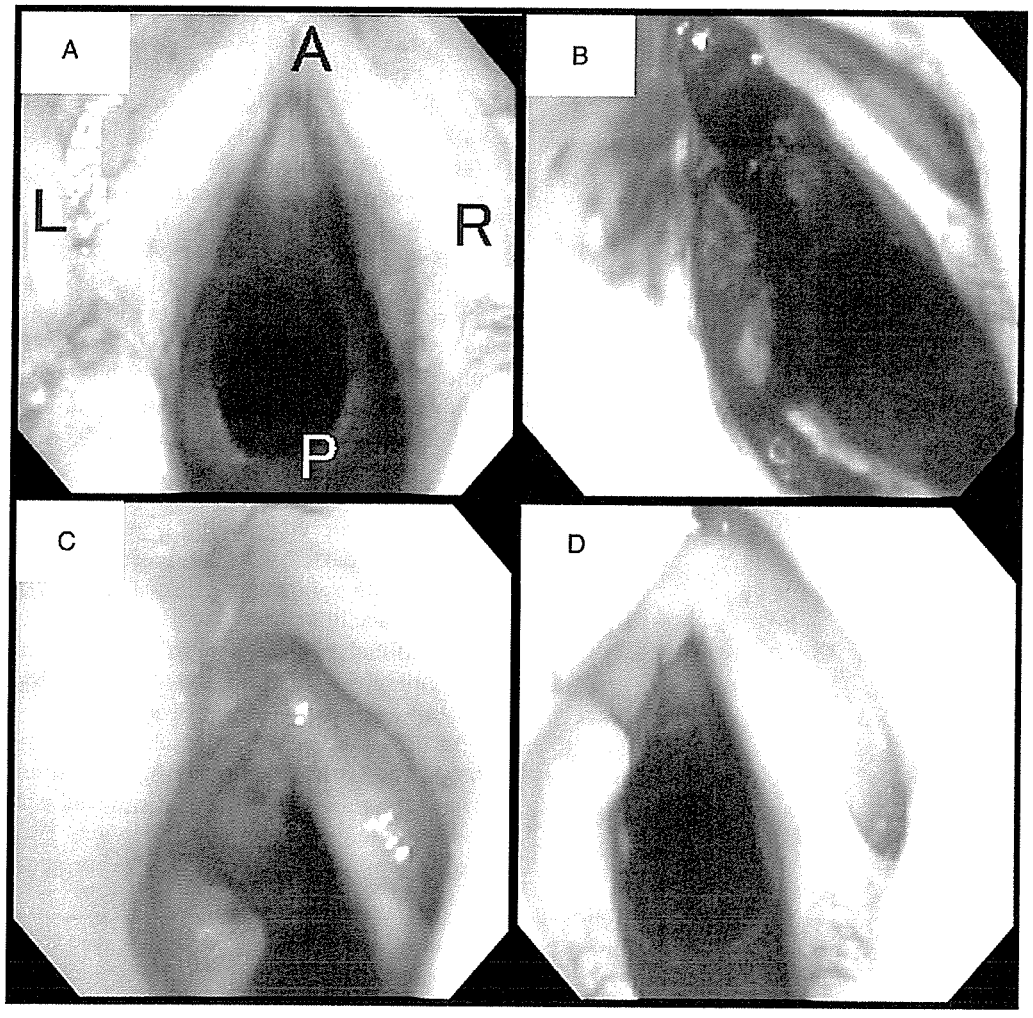

Figure 6. Endoscopic findings of canine case Z before (A), immediately after (B), day 8 (C) and 3 weeks (D) after implantation. A, anterior; P, posterior; R, right; L, left.

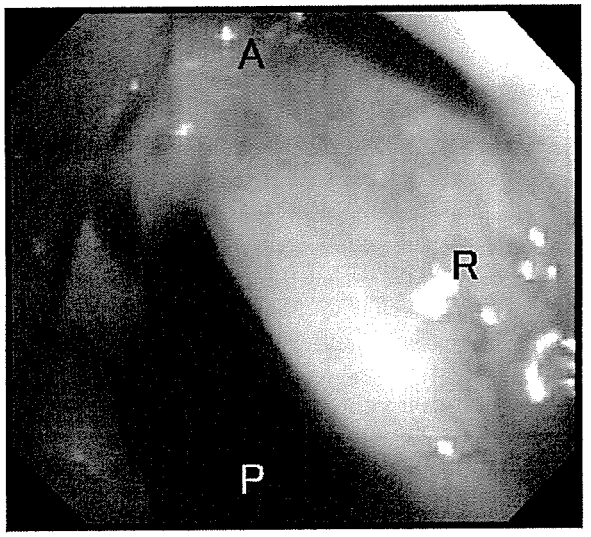

Figure 7. Endoscopic findings of canine case Z at 20 months after operation. A, anterior; P, posterior; R, right; L, left.

enhances the quality of life in patients undergoing organ reconstructions. Improved tissue engineering techniques have facilitated successful regeneration of various organs/tissues. The usual technique exploits three fundamental components: (A) cells acting as 'seeds' for tissue regeneration; (B) a scaffold where cells can proliferate and grow; and (C) regulatory factors which mediate cell behaviors.

A recent concept in in situ tissue engineering, involving the application of a porous microcellular scaffold innovated in vitro for mediating tissue repairs and regeneration processes, was proposed. This concept may allow us to omit component (A) and/or (C), which are available from surrounding tissues of the operated site.

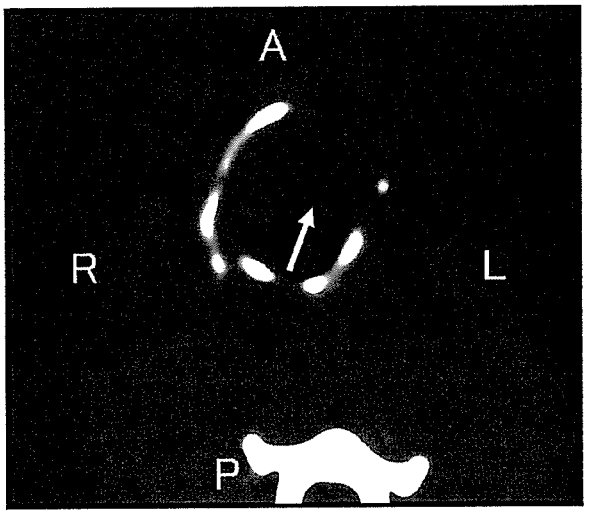

Figure 8. A CT image of canine case Z taken 15 months after implantation. The white arrow shows a bulge of the regenerated implant surface. A, anterior; P, posterior; R, right; L, left.

Our group has achieved useful outcomes in regeneration of the trachea [14,15], esophagus [16], stomach [17], and cricoid area [18] with this in situ tissue engineering technique.

Using tracheal prosthesis with porous-type collagen and polypropylene as a scaffold, Nakamura et al. [14] and Okumura et al. [15] have previously achieved favorable outcomes in canine tracheal regeneration; i.e. favorable cellular invasions of intact collagen, proper epithelialization on the luminal side of implants; and complete integration of the scaffold with the recipient's tissue were established. In addition, Omori et al. [18] have also demonstrated feasible outcomes with scaffolds containing polypropylene with spongy collagen for cricoid regeneration. In the present study, we prepared a novel scaffold using a replication of the luminal shape from a canine larynx to achieve structurally agreeable contours and improved efficacy in laryngeal reconstruction. Since polypropylene is widely used as a polymer with high biocompatibility and feasible morphological adjustability, it was appropriated as the framework material for the present novel scaffold. As polypropylene-treated scaffolds without BSCs produced unfavorable outcomes in our previous experiments, we employed BSCs in the present innovated scaffold.

Although BSCs containing mesenchymal stem cells reportedly differentiate into mesodermal tissues that eventually form muscle, bone, cartilage, etc., recent studies have revealed their potential to differentiate into other lineages such as neural [19] and epithelial tissues/structures [20,21]. The actual contributions of BSCs to the results have not been confirmed yet; however, these cells may have differentiated into epithelial cells and/or secreted certain regenerative factors.

According to Huber et al. [22], favorable outcomes in tissue engineering regeneration of canine larynx after partial hemilaryngectomy can be established with a xenogenic extracellular matrix derived from the acellular urinary bladder.

Functional recoveries with improved phonation, morphological improvement, and histological evaluations are warranted in our approach.

As the outcomes were excellent with the present cost-effective tissue engineering technique and less invasive surgical approach, our novel scaffold and regenerative technique may replace conventional surgical approaches in laryngeal reconstructions.

Conclusions

An experimental model using a scaffold infiltrated with bone marrow-derived stromal cells was innovated for laryngeal regeneration after partial resection

of the larynx. Favorable epithelialization on the scaffold with proper reconstruction of original contours was observed in one of three operated dogs. Useful outcomes and other advantageous reconstructive factors may favor the present novel tissue engineering approach over conventional surgical approaches, although further investigations are warranted to further improve the benefits and useful outcomes established so far.

References

[1] Badiavas EV, Paquette D, Carson P, Falanga V. Human chronic wounds treated with bioengineered skin: histologic evidence of host-graft interactions. J Am Acad Dermatol 2002;46:524 30.

[2] Matsumura G, Hibino N, Ikada Y, Kurosawa H, Shin'oka T. Successful application of tissue engineered vascular autografts: clinical experience. Biomaterials 2003;24:2303 8.

[3] Moroi Y, Fujita S, Fukagawa S, Mashino T, Goto T, Masuda T, et al. Clinical evaluation of allogenic cultured dermal substitutes for intractable skin ulcers after tumor resection. Eur J Dermatol 2004;14:172 6.

[4] Aubry M, Rouget J. Hemilaryngectomy with plastic reconstruction. Ann Otolaryngol 1951;68:129 39.

[5] Miodonski J, Sekula J, Olszewski E. Enlarged hemilaryngectomy (subtotal laryngectomy) with immediate reconstruction for advanced cancer of the larynx. J Laryngol Otol 1965;79:1025 31.

[6] Quinn HJ Jr. Free muscle transplant method of glottic reconstruction after hemilaryngectomy. Laryngoscope 1975;85:985 6.

[7] Park NH, Major JW Jr, Sauers PL. Hemilaryngectomy and vocal cord reconstruction with digastric tendon graft. Surg Gynecol Obstet 1982;155:253 6.

[8] Hirano M, Kurita S, Matsuoka H. Vocal function following hemilaryngectomy. Ann Otol Rhinol Laryngol 1987;96: 586 9.

[9] Delaere PR, Vander Poorten V, Vanclooster C, Goeleven A, Hermans R. Results of larynx preservation surgery for advanced laryngeal cancer through tracheal autotransplantation. Arch Otolaryngol Head Neck Surg 2000;126:1207 15.

[10] Amin MR, Koufman JA. Hemicricoidectomy for voice rehabilitation following hemilaryngectomy with ipsilateral arytenoid removal. Ann Otol Rhinol Laryngol 2001;110: 514 8.

[11] Delaere PR, Hermans R. Tracheal autotransplantation as a new and reliable technique for the functional treatment of advanced laryngeal cancer. Laryngoscope 2003;113:1244 51.

[12] Garozzo A, Rossi M. Glottic reconstruction by implant of homologous laryngeal cartilages. J Laryngol Otol 1993;107: 427 9.

[13] Kunachak S, Kulapaditharom B, Vajaradul Y, Rochanawutanon M. Cryopreserved, irradiated tracheal homograft transplantation for laryngotracheal reconstruction in human beings. Otolaryngol Head Neck Surg 2000;122:911 6.

[14] Nakamura T, Teramachi M, Sekine T, Kawanami R, Fukuda S, Yoshitani M, et al. Artificial trachea and long term follow-up in carinal reconstruction in dogs. Int J Artif Organs 2000; 23:718 24.

[15] Okumura N, Nakamura T, Natsume T, Tomihata K, Ikada Y, Shimizu Y. Experimental study on a new tracheal prosthesis made from collagen-conjugated mesh. J Thorac Cardiovasc Surg 1994;108:337 45.

[16] Hori Y, Nakamura T, Kimura D, Kaino K, Kurokawa Y, Satomi S, et al. Effect of basic fibroblast growth factor on vascularization in esophagus tissue engineering. Int J Artif Organs 2003;26:241 4.

[17] Hori Y, Nakamura T, Matsumoto K, Kurokawa Y, Satomi S, Shimizu Y. Experimental study on in situ tissue engineering of the stomach by an acellular collagen sponge scaffold graft. ASAIO J 2001;47:206 10.

[18] Omori K, Nakamura T, Kanemaru S, Kojima H, Magrufov A, Hiratsuka Y, et al. Cricoid regeneration using in situ tissue engineering in canine larynx for the treatment of subglottic stenosis. Ann Otol Rhinol Laryngol 2004;113:623 7.

[19] Neuhuber B, Gallo G, Howard L, Kostura L, Mackay A, Fischer I. Reevaluation of in vitro differentiation protocols for bone marrow stromal cells: disruption of actin cytoskeleton induces rapid morphological changes and mimics neuronal phenotype. J Neurosci Res 2004;77:192 204.

[20] Spees JL, Olson SD, Ylostalo J, Lynch PJ, Smith J, Perry A, et al. Differentiation, cell fusion, and nuclear fusion during ex vivo repair of epithelium by human adult stem cells from bone marrow stroma. Proc Natl Acad Sci U S A 2003;100: 2397 402.

[21] Song L, Tuan RS. Transdifferentiation potential of human mesenchymal stem cells derived from bone marrow. FASEB J 2004;18:980 2.

[22] Huber JE, Spievack A, Simmons-Byrd A, Ringel RL, Badylak S. Extracellular matrix as a scaffold for laryngeal reconstruction. Ann Otol Rhinol Laryngol 2003;112:428 33.

The Laryngoscope
Lippincott Williams & Wilkins, Inc.

Tracheal Regeneration After Partial Resection: A Tissue Engineering Approach

Masaru Yamashita, MD; Shin-ichi Kanemaru, MD, PhD; Shigeru Hirano, MD, PhD; Akhmar Magrufov, MD; Hisanobu Tamaki, MD; Yoshihiro Tamura, MD; Masanao Kishimoto, MD; Koichi Omori, MD, PhD; Tatsuo Nakamura, MD, PhD; Juichi Ito, MD, PhD

Objectives: **The aims of this study are to investigate the efficiency of a tissue engineering approach to partial tracheal reconstruction and to improve epithelialization of the reconstructed trachea. The trachea must be resected in some cases of cancer or trauma. Various restructuring techniques are used, with no consensus on the best approach. Two problems that arise when treating tracheal defects by conventional techniques are an inability to regenerate ciliated epithelium at the reconstructed site and having to perform multiple procedures to achieve the desired repair. This study is designed to address these problems.** ***Study Design:*** **Preliminary, an animal experiment.** ***Methods:*** **Surgery was performed on five adult beagles under anesthesia. After the making of a longitudinal cervical skin incision, the trachea was exposed and a circular defect created. A polypropylene and collagen scaffold preclotted with peripheral blood was inserted to the defect site. Postoperatively, the site was evaluated fiberscopically, histologically, and radiographically.** ***Results:*** **All dogs did well postoperatively. Fiberscopic examination showed that the implanted scaffolds were completely covered with regenerated mucosa with capillaries in all cases. Histologic data showed ciliated epithelium regenerated at the operated site from 1 month postoperatively. Newly formed cartilage was detected in the specimens from 8 to 12 postoperative months. Computed tomography images revealed the fine luminal contour of the regenerated site.** ***Conclusions:*** **Good epithelial regeneration was observed after repair of a round tracheal resection using a simple tissue engineering technique, making the technique a good substitute for conventional approaches to tracheal reconstruction in patients with cancer or trauma.** ***Key Words:*** **Tracheal regeneration, tissue engineering, polypropylene, tracheal epithelialization.**

Laryngoscope, **117:497–502, 2007**

INTRODUCTION

There are many therapeutic options for reconstructing the trachea after surgical resection following diseases such as cancer, stenosis or trauma, but no perfect way has yet been established. Primary end-to-end anastomosis is generally used for reconstruction after circumferential resection followed by stenotic lesions. It requires anastomotic tension control both intra- and postoperatively.[1,2] The "trough" method is one efficient procedure that enables the partially affected laryngotracheal region to keep an air space inside, but this requires staged and skilled operations.[3,4] Both of these conventional techniques still require improvement. Damage to the donor site or the risk of transmitted diseases from the donor should also be considered when using autologous tissue or allografts. In taking these facts into consideration, prosthetic reconstructions are preferable, although immunoreaction and tissue compatibility have to be overcome.

Remarkable progress has recently been achieved in regenerative medicine. Differentiated tissues and certain organs can now be regenerated, under appropriate conditions, using a tissue engineering technique. This technique was proposed by Langer and Vacanti[5] in 1993 and routinely requires three fundamental components: cells, scaffold, and growth-regulation factors. Of these, the scaffold on which cells are proliferated and differentiated is particularly important for regenerating structured tissues and organs. If an appropriate scaffold and conditions are prepared at the site, regeneration of the tissue would be accelerated even without implantation of cells or regulation factors.[6] Using this concept, we designed an artificial scaffold and applied it to a human case.[7] In the early postoperative period of this case, however, the luminal surface was deformed and nonepithelialized. It is very important to reduce the difference in level of the reconstructed area and to epithelialize its luminal surface at an

From the Department of Otolaryngology–Head and Neck Surgery (M.Y., S.-I.K., S.H., A.M., H.T., Y.T., M.K., J.I.), Graduate School of Medicine and the Department of Bioartificial Organs (T.N.), Institute for Frontier Medical Science, Kyoto University, Kyoto, Japan; and the Department of Otolaryngology (K.O.), Fukushima Medical University, Fukushima, Japan.

Editor's Note: This Manuscript was accepted for publication November 6, 2006.

Send correspondence to Dr. Shin-ichi Kanemaru, Department of Otolaryngology–Head and Neck Surgery, Graduate School of Medicine, Kyoto University, 54 Kawara-cho, Shogoin, Sakyo-ku, Kyoto, 6068507, Japan. E-mail: kanemaru@ent.kuhp.kyoto-u.ac.jp

DOI: 10.1097/MLG.0b013e31802e223d

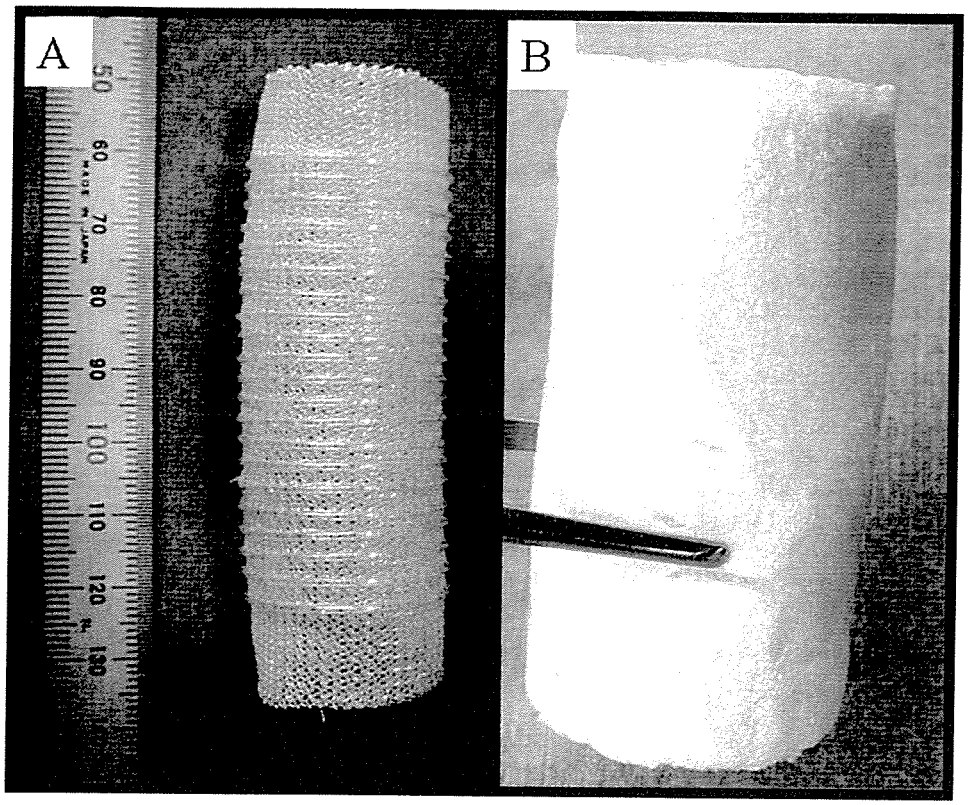

Fig. 1. (A) Polypropylene framework of artificial trachea. (B) Appearance of scaffold after spongy collagen treatment.

early postoperative stage. This study attempts to solve the problems encountered in this clinical application.

MATERIALS AND METHODS

Preparation of Scaffold and Media for Cell Growth

A single sheet of polypropylene mesh with a pore size of 260 μm (Marlex Mesh; CR Bard, Inc., Billerica, MA) was rolled and reinforced by spiral polypropylene strings (Fig. 1A). A 1% porcine dermal atelocollagen (supplied by Nippon Meatpackers, Inc., Ibaraki, Japan) preparation composed of type I (70%) and type III (30%) collagens dissolved in aqueous hydrochloric acid (pH 3.0) was used to coat both sides of this scaffold framework. This spongy collagen (Fig. 1B) would accelerate the cellular attachment and growth into the scaffold. After collagen coating, freeze drying with a freeze dryer (FDU-810, Tokyo Rikakikai Co. Ltd., Tokyo, Japan), and cross-linkage with a vacuum dry oven (VOS-300SD, Tokyo Rikakikai Co., Tokyo, Japan) were applied to the scaffold.

Animals and Surgical Procedures

Tracheal regeneration after partial resection was attempted in dogs with a revised approach, which preserved the mucosa marginally and sutured the scaffold described above to the resected site edge to edge instead of with overlaying (Fig. 2). Animal care, housing, and experimental procedures were conducted according to the Guidelines for Animal Experiments of Kyoto University. Five adult beagle dogs weighing 10 to 12 kg were anesthetized with subcutaneous (SC) injections of ketamine hydrochloride (5.0 mg/kg; Sankyo Co., Ltd, Tokyo, Japan) and xylazine hydrochloride (2.0 mg/kg; Bayer, Ltd., Tokyo, Japan) followed by tracheal intubation. The animals were then anesthetized generally with a mixture of oxygen, nitric oxide, and halothane before creation of a partial tracheal resection of 1.5 cm to 2 cm in diameter with use of a scalpel (Fig. 3A). The tracheal mucosa was preserved marginally along the cartilage defect for the acceleration of epithelialization and the prevention of scaffold dislocation.

A scaffold implant was preclotted with 5 mL of peripheral arterial blood. This resulted in the implant being completely infiltrated with blood and prevented air spaces from causing leakage. The preclotted scaffold was then trimmed to the size of the cartilage defect created during surgery and then was anastomosed to the resected boundaries of the tracheal cartilage with 3-0 absorbable sutures (Vicryl; Ethicon, Inc., Somerville, NJ) (Fig. 3B). The distance between each suture was 4 mm. Ampicillin sodium (Meiji Seika Kaisha Ltd., Tokyo, Japan) was administered (250 mg/animal; SC) for 3 days, followed by daily oral 500 mg doses for 1 week to prevent postoperative infections.

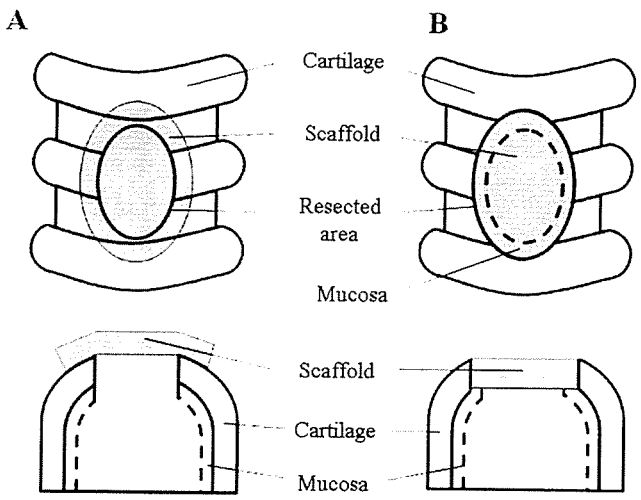

Fig. 2. Schematic of (A) our previous technique and (B) the technique described in this study.

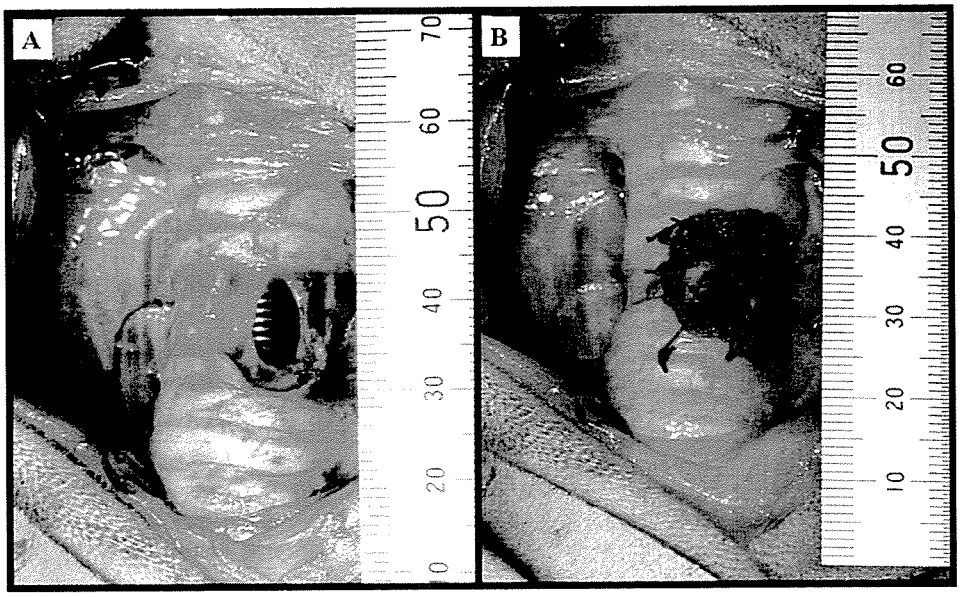

Fig. 3. (A) Patch defect approximately 1.5 cm in diameter was created on cervical trachea by scalpel. (B) Scaffold preclotted with peripheral arterial blood was trimmed and fixed to defect boundaries with bioabsorbable sutures.

Outcome Assessment

Endoscopic examinations to monitor progress of regenerative status were undertaken periodically with a video-endoscopy system consisting of a video bronchoscope (BF type 1T240, Olympus Co., Tokyo, Japan) and a video processor (CV-240, Olympus Co., Tokyo, Japan) with a light source (CLV-U40D, Olympus Co., Tokyo, Japan). Anesthesia was induced with ketamine hydrochloride and xylazine hydrochloride (see above) to facilitate these examinations.

Histologic assessments including light microscopy and scanning electron microscopy were also performed to evaluate the regenerative status of the operated site at various time points up until 1 year postoperatively. One year postoperatively, a three-dimensional image of a dog's trachea was obtained using computed tomography (CT) performed on the operated site using a helical CT scanner system (Legato Duo, GE Yokogawa Medical Systems, Tokyo, Japan).

RESULTS

The postoperative conditions of all dogs were good. None of them showed any signs of infection. Local fiberscopic findings from the five dogs showed no stenosis or

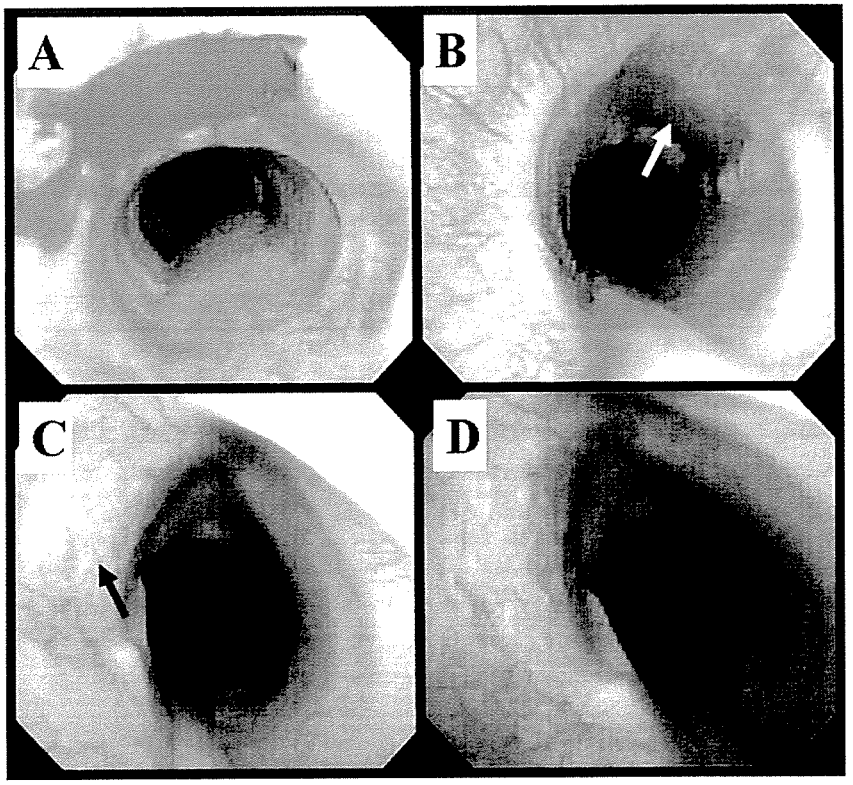

Fig. 4. (A) Preclotted and fixed scaffold implant was a good-fit on tracheal defect in a dog. (B) Implant surface was covered with soft tissues on day 7 after operation. Images 6 months (C) and 1 year (D) after operation in another dog. Implant was completely covered with regenerated mucosa without any granulation or displacement. Good vascularization was also observed in both images.

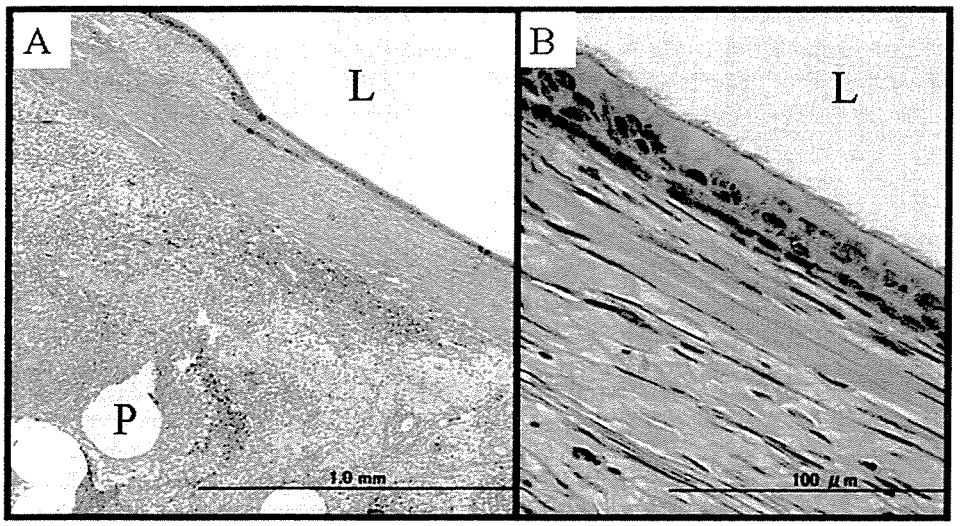

Fig. 5. Hematoxylin-eosin stained images of tissue from central portion of regenerated site 1 month after operation. (A) Many inflammatory cells are seen in submucosa. Luminal surface is completely covered with epithelial cells on layered connective tissue. (B) Ciliated epithelium is clearly observed, although concentration of cilia is low (magnification ×200). L = tracheal lumen; P = polypropylene.

granulation in the regenerated trachea. The implanted scaffolds were completely covered with newly regenerated mucosa with capillaries in all cases.

Figure 4 shows the fiberscopic images from operated dogs with typical luminal portrayal of a successfully reconstructed trachea 1 year postoperatively (Fig. 4D) compared with the tracheal image obtained just after surgery (Fig. 4A). The preclotted and fixed scaffold implant was a good fit on the tracheal defect, and the implant surface was covered with soft tissues on day 7 after surgery (Fig. 4B). Figure 4C and 4D, taken at 6 months and 1 year after surgery, respectively, show that the implant was completely covered with regenerated mucosa without any granulation or dislocation of the scaffold.

Histologic assessments reveal infiltration by many inflammatory cells around the polypropylene framework 1 month after surgery (Fig 5A). The epithelial lining was already complete at the operated site, although the concentration of cilia was low (Fig 5B).

Eight months after surgery, a fine, complete epithelial lining with newly formed immature cartilage and pseudo-ossification was detected (Fig. 6), and proliferation of ciliated epithelial cells with subepithelial glands was observed in light microscopic images (Fig. 7). A scanning electron microscopic image of regenerated cilia is shown in Figure 8. No inflammatory reaction was found in any of the specimens 8 months after surgery. A summary of histologic data is shown in Table I. One year after surgery, axial CT images at the operated sites revealed a fine luminal portrayal of the reconstructed trachea (Fig. 9A), but no obvious cartilage signal was detected in the three-dimensional images reconstructed from fine axial images (Fig. 9B).

DISCUSSION

Various treatment options to reconstruct the trachea after partial surgical resections or structural damage have been pursued for more than 50 years.[8] However, established treatments have remained controversial as surgeons continue to encounter inconsistent outcomes in tracheal reconstructions. Factors contributing to unsatisfactory outcomes include 1) lack of ciliated epithelium, which contributes to autopurification; 2) infection or foreign body reaction;

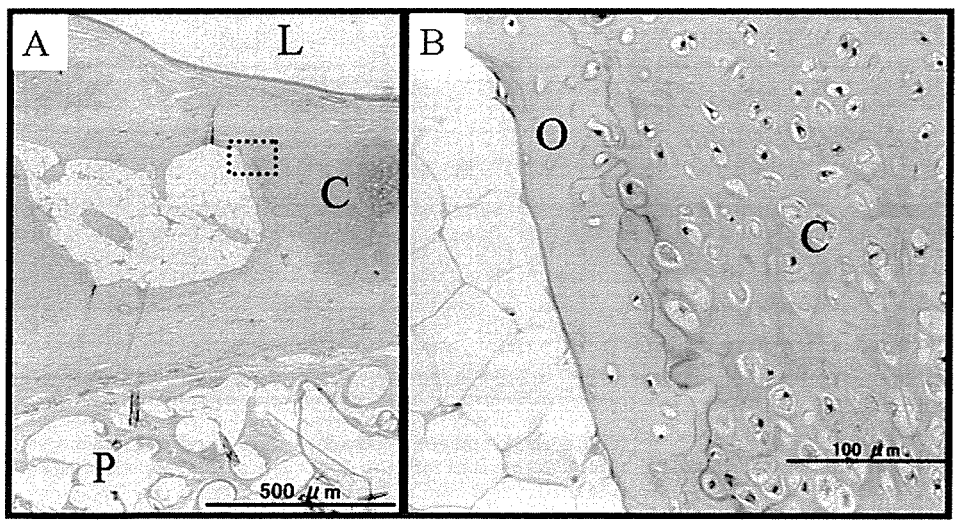

Fig. 6. Histologic images of regenerated tissue 8 months after surgery (hematoxylin-eosin). (A) Luminal surface is covered with epithelium, and an area with newly formed immature cartilage and pseudo-ossification is indicated by dotted area. Polypropylene framework of scaffold is on outer side. (B) Magnification (×100) of dotted area in A; regenerated cartilage with chondrocytes and pseudo-ossification are seen. L = tracheal lumen; C = cartilage; P = polypropylene; O = pseudo-ossification.

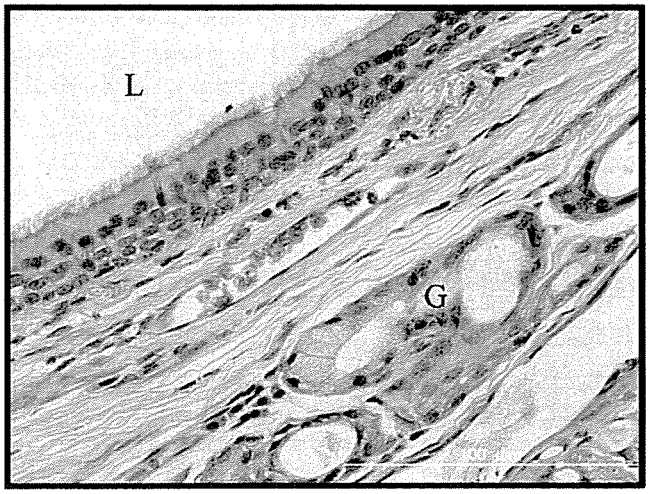

Fig. 7. Microscopic image of regenerated epithelium 8 months after surgery (hematoxylin-eosin). Proliferation of stratified ciliated epithelial cells with subepithelial glands observed. L = tracheal lumen; G = gland.

and 3) repeated surgeries including tracheostomy. Although autologous tissues[9] and homografts[10] have hitherto been used as implant materials for tracheal reconstruction, damage inflicted on the donor site or the risk of donor-recipient disease transmissions warrant a more clinically efficient approach. Moreover, in cases with tumors invading into the trachea, deformities of the reconstructed site render it difficult to monitor the tumor recurrence. Furthermore, unintentionally inflicted cosmetic handicaps in postoperated patients sometimes result in unfavorable psychologic outcomes that eventually defeat the reconstruction effort. A regenerative approach for this area is suitable to overcome these problems.

Regenerative medicine has recently been accepted as a useful clinical discipline that ensures and enhances the quality of life in patients undergoing organ reconstructions. Improved tissue engineering techniques have facilitated successful regenerations of various organs/tissues.

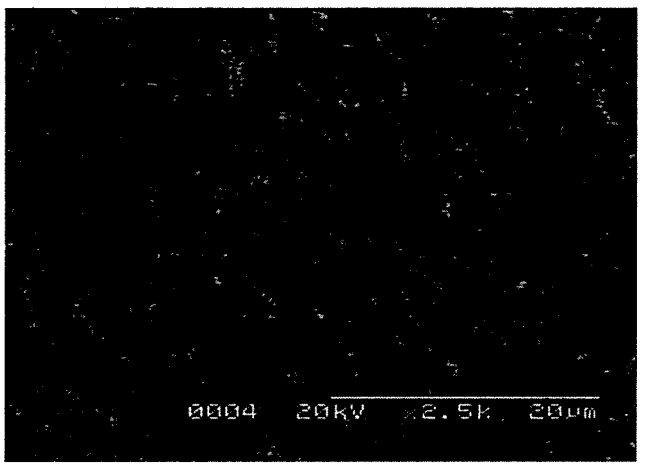

Fig. 8. Scanning electron microscopic image on luminal surface of scaffold. Well-regenerated cilia covers luminal surface of scaffold.

TABLE I.
Summary of Histologic Data.

Months	1	8	10	12
Epithelialization	+	+	+	+
Gland	—	+	+	+
Inflammatory cells	+	—	—	—
Cartilage	—	+	+	+

These techniques rely on three fundamental components: 1) cells acting as "seeds" for tissue regeneration; 2) scaffolds where cells can proliferate and grow; and 3) regulatory factors that mediate cell behaviors. A recent concept in in situ tissue engineering, involving the application of an in vitro innovated porous microcellular scaffold for mediating tissue repair and regeneration processes, has been proposed. Under suitable conditions, this concept would allow for the omission of component 1 or 3 or both, which would be available from tissues surrounding the operated site. Our group has been successful in regeneration of mastoid air cells,[11] cricoid area,[12] and nerves[13,14] solely by using scaffolds.

In the present study, we prepared a novel scaffold made of polypropylene and dermal collagen from porcine skin to regenerate the functional trachea after creating a partial tracheal defect. Because polypropylene is widely used as a polymer with high biocompatibility and feasible morphologic adjustability, it was appropriate for use as the framework material for this novel scaffold.

Using this tracheal prosthesis with porous-type collagen and polypropylene as a scaffold, Okumura et al.[15] have previously achieved favorable outcomes in canine circumferential tracheal regeneration, namely, favorable cellular invasion to intact collagen, proper epithelialization on the luminal side of implants, and complete integration of the scaffold with the recipient's tissue. In the clinic, not many patients require this circumferential resection. Especially in cases of head and neck malignancies, injury to the trachea is usually limited to the wall; therefore, partial tracheal resections are the procedures most frequently performed. Thus, the experimental setup of this study is more appropriate.

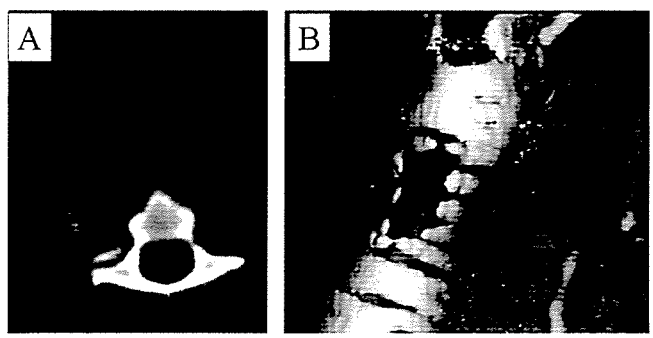

Fig. 9. (A) Axial computed tomography image at operated site reveals fine luminal portrayal of reconstructed trachea. (B) Three-dimensional reconstructed image from fine axial sections shows no marked new cartilage formation.